Progress In Electromagnetics Research, Vol. 108, 141–153, 2010

A DUAL-WIDEBAND BANDPASS FILTER BASED ON E-SHAPED MICROSTRIP SIR WITH IMPROVED UPPER-STOPBAND PERFORMANCE

Y.-L. Wu, C. Liao, and X.-Z. Xiong

Institute of Electromagnetics
Southwest Jiaotong University
Chengdu 610031, China

Abstract—A novel dual-wideband microstrip bandpass filter (BPF) with improved upper-stopband performance is presented. With the use of some special structures such as E-shaped microstrip Stepped-Impedance Resonator (SIR) and input-output cross-coupling feed structure, this filter can generate five transmission zeros which are beneficial for improving its frequency selectivity and upper-stopband performance. Finally the microstrip dual-wideband BPF has been simulated, fabricated and measured. Measurement results show that the two passbands are centered at 3.7 GHz and 5.8 GHz with the fractional bandwidth of 31% and 13% respectively. Meanwhile more than 50% relative upper-stopband bandwidth with 20 dB rejection has been realized. The simulated and measured results are in good agreement.

1. INTRODUCTION

With the developments of wireless communication systems there are more and more demands for dual-band microwave filters. The concept of dual-band filter was initially introduced by directly cascading two individual filters with two specified single bands [1]. Recently, a number of publications have provided a variety of solutions to the realization of dual-band bandpass filter [2–9]. In [2], a dual-band BPF is achieved by loading distributed capacitors in the inner area of conventional dual-mode loop resonator. In [3], frequency transformation technique is employed to determine the locations of

Received 18 July 2010, Accepted 6 September 2010, Scheduled 14 September 2010
Corresponding author: Y.-L. Wu (wyljd@sina.com).

poles and zeros of a desired dual-band BPF. Dual-band filters can also be realized by using meander-loop resonators [4, 5]. Besides utilizing meander-loop resonators, a dual-band filter can also be realized by using microstrip open-loop resonators or hybrid other resonator structures [6–9]. Stepped impedance resonators (SIRs) are suitable for the dual-band filter design because the spurious frequency response can be used to create the second passband for dual-passband response [10–13]. However, most of the aforementioned dual-band filters are basically appropriate for the design of narrow bands (fractional bandwidth less than 10%) and dual-band BPFs with wide bandwidth received fewer reports [15]. Liu et al. [14] used a frequency mapping approach to design dual-wideband BPFs with SIRs. Chin and Yeh [15] utilized a short-circuited stepped-impedance resonator to achieve dual-wideband capability and minimum size. The composite microstrip and CPW structure were proposed in [16] to design dual-wideband filters. Ladder stub resonator (LSR) structure is also proposed to design dual-wideband filter in [17]. In [18], a dual-wideband BPF is achieved by using resonators based on slotted ground structures. Nevertheless, all the dual-wideband BPFs in [14–18] are still embarrassed by the existence of a very narrow upper-stopband, even a poor lower-stopband. Although there are already some on the expansion of the upper-stopband reports [19–21], they are basically based on a single passband bandpass filter.

In this article, a dual-wideband filter whose five transmission zeros are distributed in the lower, middle and upper stopbands has been realized by the use of a E-shaped microstrip stepped-impedance resonator (SIR) and a cross-coupling structure between the input and output feed lines [22–25]. Whose frequency response characteristics exhibit sharp roll-off that should improve the edge performance of the passband and stopband. Meanwhile the different frequency responses can be obtained by changing the positions of the five transmission zeros, i.e., adjusting the geometric dimensions of the E-shaped SIR and input-output cross-coupling feed structure.

The proposed dual-wideband filter has been constituted, designed and fabricated. The dimensions of the proposed filter are 24 mm $\times$ 15 mm if the length of the feed lines is ignored. Compared to the reported filters [14–18] the measured results of this proposed filter give much better upper-stopband performance. Meanwhile, the dual-wideband filter shows excellent lower-stopband performance.

2. STRUCTURE AND ANALYSIS OF THE DUAL-WIDEBAND MICROSTRIP BPF

The E-shaped SIR has been used in this novel dual-wideband filter. As shown in Fig. 1(a), the E-shaped SIR consists of three high-impedance microstrip open-circuited stubs which are shunt to a low-impedance microstrip line. The left microstrip open-circuited stub is the same as the right one. Therefore, the E-shaped microstrip SIR resonator is symmetric with respect to the middle-axes. The basic structure of a microstrip SIR is shown in Fig. 1(b). It consists of three serial transmission line sections with two different characteristic impedances. The middle one has a longer electric length ($2\theta_1$) and lower impedance (Z_1). Meanwhile, both side sections have relatively shorter electric lengths (θ_2) and higher impedances where the impedance ratio may be defined as $K = Z_2/Z_1 = Y_1/Y_2 > 1$ and $\theta_T > \pi$ [26]. The admittance of the resonator from the open end, Y_{in}, is given as

$$Y_{in} = jY_2 \cdot \frac{2(K\tan\theta_1 + \tan\theta_2)\cdot(K - \tan\theta_1\cdot\tan\theta_2)}{K(1-\tan^2\theta_1)\cdot(1-\tan^2\theta_2) - 2(1+K^2)\cdot\tan\theta_1\cdot\tan\theta_2} \quad (1)$$

The resonance condition can be obtained from the following:

$$Y_{in} = 0 \quad (2)$$

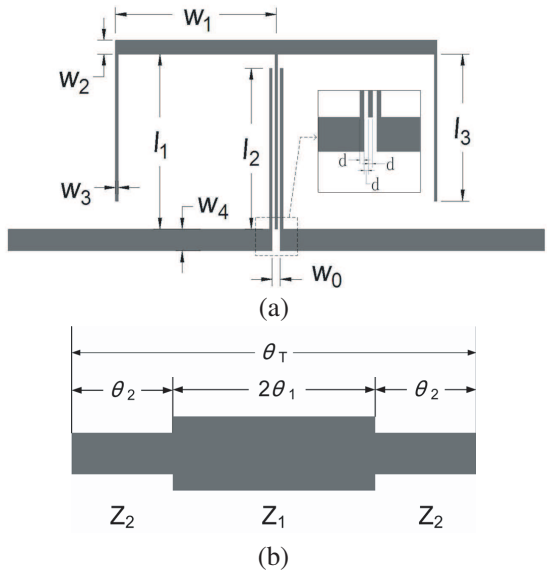

Figure 1. (a) Layout of proposed dual-wideband E-shaped SIR BPF. (b) Structure of the SIR, where $K = Z_2/Z_1 > 1$ and $\theta_T > \pi$.

From (1) and (2) the fundamental resonance condition can be expressed as

$$K = \tan\theta_1 \cdot \tan\theta_2 \tag{3}$$

For practical application it is preferable to choose $\theta_1 = \theta_2 = \theta$ because the design equations can be simplified considerably, and (1) can be expressed as

$$Y_{in} = jY_2 \frac{2(1+K)\cdot(K-\tan^2\theta)\cdot\tan\theta}{K-2(1+K+K^2)\cdot\tan^2\theta+K\tan^4\theta} \tag{4}$$

The resonance condition is then given, using the fundamental frequency f_{m1} and corresponding electric length θ_1, as

$$\tan^2\theta_1 = K \quad \text{or} \quad \theta_1 = \arctan\sqrt{K} \tag{5}$$

Taking the spurious resonance frequency to be f_{m2}, f_{m3}, f_{m4} and corresponding electric length with θ_2, θ_3, θ_4, we can obtain from (4) and (2)

$$\begin{aligned} &\tan\theta_2 = \infty \\ &\tan^2\theta_3 - K = 0 \\ &\tan\theta_4 = 0 \end{aligned} \tag{6}$$

Then

$$\begin{aligned} \frac{f_{m2}}{f_{m1}} &= \frac{\theta_2}{\theta_1} = \frac{\pi}{2\arctan\sqrt{K}} \\ \frac{f_{m3}}{f_{m1}} &= \frac{\theta_3}{\theta_1} = 2\left(\frac{f_{m2}}{f_{m1}}\right) - 1 \\ \frac{f_{m4}}{f_{m1}} &= \frac{\theta_4}{\theta_1} = 2\left(\frac{f_{m2}}{f_{m1}}\right) \end{aligned} \tag{7}$$

It is clear from (7) that all the spurious response can be controlled by the characteristic impedance ratio K. In this design, considering that $K = 2$ and $f_{m1} = 3.7\,\text{GHz}$, the frequency ratio f_{m2}/f_{m1}, f_{m3}/f_{m1}, f_{m4}/f_{m1} can be determined as nearly 1.6, 2.3, 3.3, respectively. In order to further adjust the spurious passbands, we introduce input-output cross-coupled feed structure and add a high-impedance open stub to the SIR to form an E-shaped SIR [27]. Fig. 3 shows the simulated frequency response of the E-shaped SIR under different section lengths. It can be seen that the results of theoretical analysis and full-wave simulation are in good agreement when f_{m1}, f_{m2}, f_{m3}, and f_{m4} distribute around 3.7, 5.6, 9.3, and 12.5 GHz, respectively.

To obtain much tighter coupling between the input/output ports and E-shaped SIR, the input-output cross-coupled feed structure was

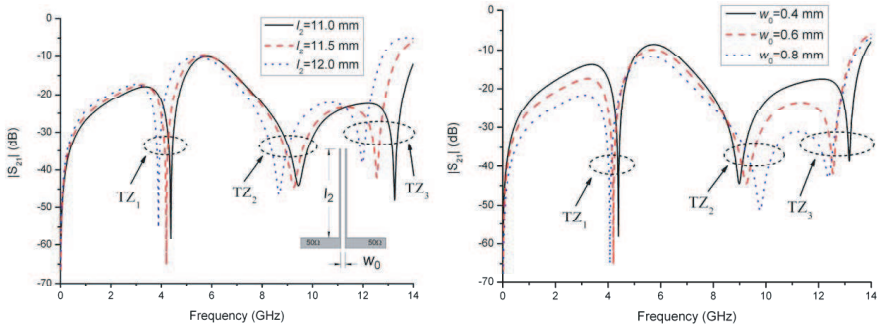

(a) (b)

Figure 2. Simulated S_{21} magnitude of the input-output cross-coupling feed structure. (a) Fixed $w_0 = 0.6\,\text{mm}$, and varied l_2. (b) Fixed $l_2 = 11.5\,\text{mm}$, and varied w_0.

proposed in this filter. As shown in Fig. 2(a), this feed structure is formed by attaching two high-impedance microstrip open-circuited stubs shunt to the input/output microstrip lines, respectively.

Figure 2(a) shows the simulated magnitude of S_{21} of this coupling structure with fixed $w_0 = 0.6\,\text{mm}$ and different l_2. It can be seen that this feed structure has three transmission zeros, namely, TZ_1, TZ_2 and TZ_3. As l_2 increases from 11 mm to 12 mm, TZ_1, TZ_2 and TZ_3 all move towards the low frequencies, the moving range of TZ_1 less than those of TZ_2 and TZ_3. On the other hand, as shown in Fig. 2(b), if fixing $l_2 = 11.5\,\text{mm}$ and increasing w_0, TZ_1 and TZ_3 still move towards the low frequencies, but the TZ_2 shifts to higher frequencies. The shifting range of TZ_1 is smaller than those of TZ_2 and TZ_3. Thus, we can see that the first transmission zero TZ_1 may be adjusted to between the two passbands. Meanwhile, the second transmission zero TZ_2 and the third transmission zero TZ_3 may be allocated among the upper-stopbands to provide better edge behaviors as well as improved upper-stopband performance.

The frequency-dependent transmission response of the presented E-shaped SIR under the weak coupling case ($l_2 = 0.5\,\text{mm}$) is shown in Fig. 3. It can be seen that there are four main resonant modes, f_{m1}, f_{m2}, f_{m3}, f_{m4}, in the range of 3.0–14.0 GHz. The configuration of the proposed E-shaped SIR is shown in Fig. 3(a). There are three adjustable variables, i.e., w_1, l_1, l_3. As shown in Fig. 3(b), the second resonant mode f_{m2} shifts downwards slightly, and the fourth resonant mode f_{m4} sways around 12.5 GHz as the stub length l_1 is increased from 12, 12.5 to 13 mm. Meanwhile, the first and third resonant modes, f_{m1} and f_{m3}, remain stationary. It is valid in theory that the center location

of the resonator corresponds to a short circuit or perfect electrical wall for odd modes, and its characteristics are hardly affected by the attachment of the shunt stub l_1, whereas it indicates an open circuit or perfect magnetic wall for all the even resonant modes [28]. Thus, the second mode can be adjusted to the middle of the second passband, while the fourth mode can be raised and allocated away from the second passband.

In addition, as shown in Fig. 3(c), the third and fourth resonant modes, f_{m3}, f_{m4}, move towards the lower frequencies quickly, the resonant modes f_{m1}, f_{m2} remaining almost unchanged, while changing the w_1 from 11 mm to 13 mm. Furthermore, as shown in Fig. 3(d), the resonant modes f_{m1}, f_{m2} move downwards slightly, and the resonant mode f_{m3} shifts downwards quickly, but the fourth mode f_{m4} sways around 12.5 GHz, when the stub length l_3 is increased from 9.5 mm to

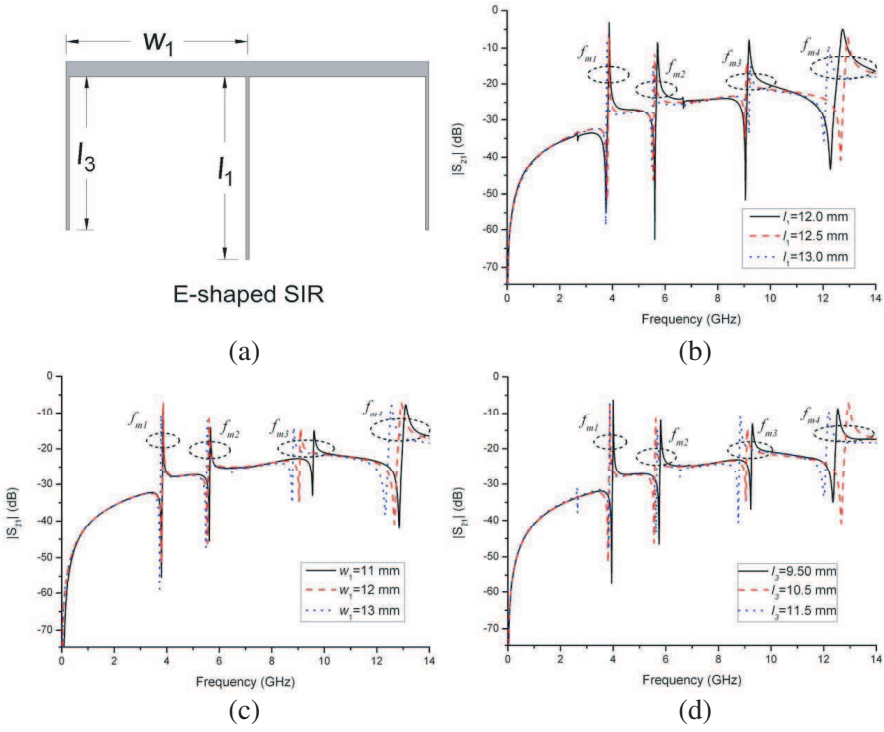

Figure 3. Simulated frequency-dependent transmission responses of the presented E-shaped SIR. (a) Configuration of proposed E-shaped SIR. (b) Fixed $w_1 = 12$ mm, $l_3 = 10.5$ mm and varied l_1. (c) Fixed $l_1 = 12.5$ mm, $l_3 = 10.5$ mm and varied w_1. (d) Fixed $w_1 = 12$ mm, $l_1 = 12.5$ mm and varied l_3.

11.5 mm. Therefore, the two side impedance-stepped stubs with varied w_1, l_3 can provide additional degrees of freedom to adjust the locations of the four resonant modes in alternative ways.

Based on the above discussion, the first two resonant modes (f_{m1}, f_{m2}) can be used to construct dual-wideband passbands, if the E-shaped SIR is properly fed with input-output cross-coupling feed structure. In addition, it can be seen that the third resonant mode f_{m3} of E-shaped SIR is highly rejected by the second transmission zero TZ_2 of the input-output cross-coupling feed structure at around 9.3 GHz, as shown in Fig. 4(a). However, as aforementioned, the fourth resonant mode f_{m4} of E-shaped SIR is always swaying around 12.5 GHz in most cases. For this reason, it is hardly suppressed by adjusting the third transmission zero TZ_3 of the feed structure while performance of the dual-wideband BPF must be guaranteed. Finally, we choose $l_1 = 12.5$ mm, $w_1 = 12$ mm, $l_3 = 10.5$ mm. As a result, a dual-wideband BPF with improved upper-stopband is realized (with insertion loss larger than 20 dB in the range of 6.9 to almost 12 GHz in measurement).

Figure 4(a) shows the simulated frequency response of the filter with fixed $l_1 - l_3 = 2$ mm, $l_1 - l_2 = 1$ mm and tuning the length of l_1. It is clearly observed that two passbands both move downwards when l_1 increases from 11.5 mm to 12.5 mm. On the other hand, as shown in Fig. 4(b), the bandwidth of the first passband increases, and the bandwidth of second passband reduces as the length of l_3 reduces from 11 mm to 10 mm. From the above discussion we can change the operating frequency of each passband flexibly through varying the length of l_1 and l_3. Moreover, as mentioned earlier we can also change

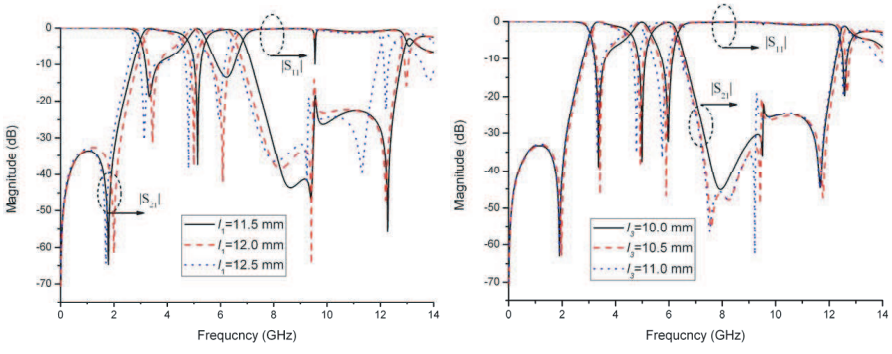

(a) (b)

Figure 4. Simulated frequency response of the proposed filter. (a) Fixed $l_1 - l_3 = 2$ mm, $l_1 - l_2 = 1$ mm and varied l_1. (b) Fixed $l_1 = 12.5$ mm and varied l_3.

two passbands frequencies with altering characteristic impedance ratio K. It is clear from (7) that the center frequency of second passband (f_{m2}) will be away from the center frequency of the first passband (f_{m1}) as K reduces. On the contrary, f_{m2} will be close to f_{m1} when K increases.

3. SIMULATED AND MEASURED RESULTS

According to the above analysis, the proposed dual-wideband BPF is designed, simulated, and optimized by using a full wave finite element method simulator. The final dimensions of the filter are as follows: $w_0 = 0.6\,\text{mm}$, $w_1 = 12\,\text{mm}$, $w_2 = 1\,\text{mm}$, $w_3 = 0.2\,\text{mm}$, $w_4 = 1.55\,\text{mm}$, $l_1 = 12.5\,\text{mm}$, $l_2 = 11.5\,\text{mm}$, $l_3 = 10.5\,\text{mm}$, $d = 0.2\,\text{mm}$. Using a print-circuit-board (PCB) technique, the filter was fabricated on the Rogers RT/duroid 5880 substrate with dielectric constant $\varepsilon_r = 2.2$, loss tangent $\tan\delta = 0.0009$, and thickness of 0.508 mm, and the fabricated dual-wideband E-shaped SIR filter with attached SMA connectors is shown in Fig. 5. Although a low dielectric constant substrate has been used, if the feedlines are ignored, the size of the filter is only $24\,\text{mm} \times 15\,\text{mm}$, i.e., $0.39\lambda_g \times 0.25\lambda_g$, where λ_g is the guided wavelength at the centre frequency of the lower passband.

The dual-wideband E-shaped SIR BPF was measured on an Agilent E5071C ENA series Network Analyzer. The simulated and measured results of the fabricated dual-wideband BPF at the frequency range 300 KHz–14 GHz are shown in Fig. 6. Simulated results of the dual-wideband bandpass filter show that there are two passbands whose center frequencies are 3.7 and 5.8 GHz, and 3 dB fractional bandwidths are 46% and 20%, respectively. However, the measured results show that there are also two passbands at the central frequencies of 3.7 and 5.8 GHz, but the 3 dB fractional bandwidths are altered to be 31% and 13%, respectively. These minor discrepancies between

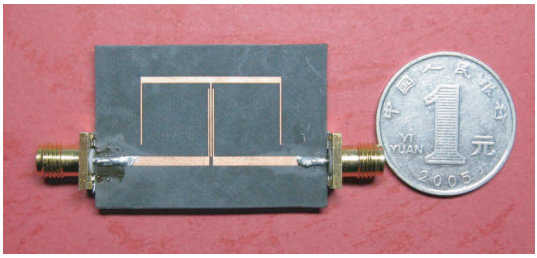

Figure 5. Photograph of fabricated dual-wideband BPF.

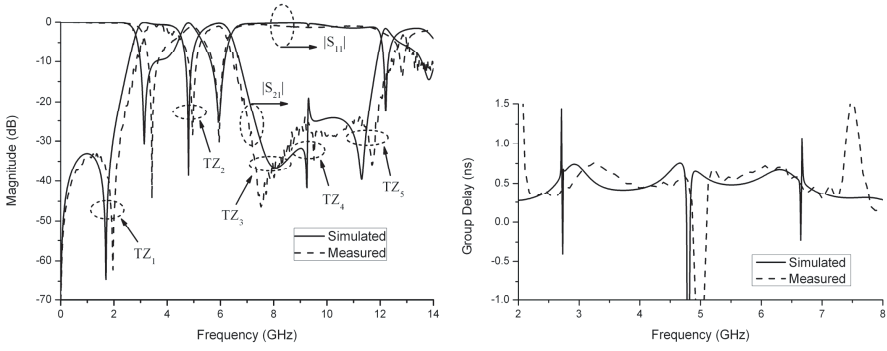

Figure 6. Simulated and measured frequency responses of the proposed dual-wideband BPF. (a) S_{21} and S_{11} magnitudes. (b) Group delay.

simulated and measured results should be caused by insertion loss of SMA connectors and unexpected tolerances in fabrication, material parameters and soldering etc. Excluding the influence of these factors. The simulated and measured results show good agreement. As shown in Fig. 6(a), for the first and second passbands at 3.43, 5.95 GHz the measured insertion loss is less than 0.7, 1 dB, and the return loss is greater than 40 and 30 dB respectively. The rejection between the two transmission bands is more than 25 dB. The measured group delay varies between 0.45 and 0.76 ns with a maximum variation of 0.31 ns from 3.1 GHz to 4.2 GHz. In the second passband, the measured group delay varies between 0.54 and 0.72 ns with a maximum variation of 0.18 ns from 5.4 GHz to 6.2 GHz.

Moreover, it can be seen from Fig. 6(a) that there are five transmission zeros which are located at 1.96, 4.95, 7.53, 9.51 and 11.7 GHz respectively, namely, from TZ_1 to TZ_5. According to our analysis transmission zeros TZ_1 and TZ_4 are produced by source-loading cross coupling. TZ_2 is the transmission zero of the E-shaped SIR, and TZ_3 and TZ_5 are caused by the interacting of source-loading cross-coupling structure and E-shaped SIR. Significantly, transmission zeros TZ_1 and TZ_3 locate at the lower and upper sides of the two passbands with attenuation more than 60 and 45 dB respectively. Meanwhile, they exhibit sharp roll-off at the two edges of the two passbands. Further, transmission zero TZ_2 is in the middle of the two passbands, which may greatly improve the isolation of the two passbands. We can see that the rejection level of the two passbands is more than 25 dB. As shown in Fig. 6(a), transmission zeros TZ_4 and

TZ_5 are distributed in the upper-stopband region. Thus, it can be seen that spurious high-frequency bands are suppressed to be below −20 dB for the frequency up to almost 12 GHz, and this is better than other reported dual-wideband filters [14–18]. For comparison, Table 1 summarizes some dual-wideband BPFs performance, where the 20 dB relative upper-stopband bandwidth (RSB) is given by

$$RSB = \frac{upper - stopband\ bandwidth}{upper - stopband\ centre\ frequency} \times 100\% \qquad (8)$$

Based on the above discussion, it can be seen that the proposed filter topology features a wider upper-stopband bandwidth (53.7%) among these filters, at the same time has an excellent lower-stopband performance. Furthermore, the proposed filter has relatively small area in comparison with previous works. However, the passbands bandwidth of this work is comparative narrow, which might be improved in future study.

Table 1. Performance comparisons among published filters and proposed one.

Ref.	Circuit size (λ_g*)	Fractional bandwidths	20 dB absolute lower-stopband range (GHz)	20 dB relative upper-stopband bandwidth (RSB)
$[14]_1$	1.07×0.36	50%/28.1%	0–0.68	35.6%
$[14]_2$	1.27×0.35	47.6%/48.4%	0–2.5	18.6%
[15]	0.3×0.3	50%/20%	0–0.55	6.7%
[16]	0.75×0.54	36%/35%	2.98–3.86	5.5%
[17]	0.51×0.42	41.5%/25.7%	2.4–2.8	4.2%
[18]	0.17×0.14	37.6%/27%	0–1.7	0.02%
This work	0.39×0.25	31%/13%	0–2.53	53.7%

$*\lambda_g$ is the guided wavelength at the centre frequency of the lower passband.

4. CONCLUSIONS

In this paper, a novel dual-wideband BPF based on E-shaped microstrip SIR structure and input-output cross-coupling feed structure has been investigated. The simulated and measured results show that the E-shaped dual-wideband SIR BPF has the advantages

of excellent lower-stopband, upper-stopband performance and good frequency selectivity. In addition, it exhibits the property of a wide dual-passband.

ACKNOWLEDGMENT

This work was supported by the Open Research Fund of Key Laboratory of Cognitive Radio and Information Processing of Ministry of Education of China, and by the National Natural Science Foundation of China under Grant 11076022.

REFERENCES

1. Miyake, H., S. Kitazawa, T. Ishizaki, T. Yamada, and Y. Nagatom, "A miniaturized monolithic dual band filter using ceramic lamination technique for dual mode portable telephones," *IEEE MTT-S Int. Dig.*, Vol. 2, 789–792, June 1997.
2. Wang, J.-P., L. Wang, Y.-X. Guo, Y. X. Wang, and D.-G. Fang, "Miniaturized dual-mode bandpass filter with controllable harmonic response for dual-band applications," *Journal of Electromagnetic Waves and Applications*, Vol. 23, No. 11–12, 1525–1533, 2009.
3. Li, G., B. Wu, X. W. Dai, and C. H. Liang, "Design techniques for asymmetric dual-passband filters," *Journal of Electromagnetic Waves and Applications*, Vol. 22, No. 2–3, 375–383, 2008.
4. Wu, G.-L., W. Mu, X.-W. Dai, and Y.-C. Jiao, "Design of novel dual-band bandpass filter with microstrip meander-loop resonator and CSRR DGS," *Progress In Electromagnetics Research*, Vol. 78, 17–24, 2008.
5. Dai, X.-W., C.-H. Liang, G. Li, and Z.-X. Chen, "Novel dual-mode dual-band bandpass filter using microstrip meander-loop resonators," *Journal of Electromagnetic Waves and Applications*, Vol. 22, No. 4, 573–580, 2008.
6. Dai, X.-W., C.-H. Liang, B. Wu, and J. W. Fan, "Novel dual-band bandpass filter design using microstrip open-loop resonators," *Journal of Electromagnetic Waves and Applications*, Vol. 22, No. 2, 219–225, 2008.
7. Zhang, L., Z.-Y. Yu, and S.-G. Mo, "Dual-mode dual-band bandpass filter using an new open-loop resonator," *Journal of Electromagnetic Waves and Applications*, Vol. 23, No. 11–12, 1603–1609, 2009.

8. Lin, H.-J., X. Q. Chen, X. W. Shi, L. Chen, and C. L. Li, "A dual passband filter using hybrid microstrip open loop resonators and coplanar waveguide slotline resonators," *Journal of Electromagnetic Waves and Applications*, Vol. 24, No. 1, 141–149, 2010.
9. Lai, X., N. Wang, B. Wu, and C.-H. Liang, "Design of dual-band filter based on OLRR and DSIR," *Journal of Electromagnetic Waves and Applications*, Vol. 24, No. 2–3, 209–218, 2010.
10. Velazquez-Ahumada, M. D. C., J. Martel-Villagr, F. Medina, and F. Mesa, "Application of stub loaded folded stepped impedance resonators to dual band filter design," *Progress In Electromagnetics Research*, Vol. 102, 107–124, 2010.
11. Weng, M. H., C. H. Kao, and Y. C. Chang, "A compact dual-band bandpass filter with high band selectivity using cross-coupled asymmetric sirs for wlans," *Journal of Electromagnetic Waves and Applications*, Vol. 24, No. 2–3, 161–168, 2010.
12. Alkanhal, M. A. S., "Dual-band bandpass filters using inverted stepped-impedance resonators," *Journal of Electromagnetic Waves and Applications*, Vol. 23, No. 8–9, 1211–1220, 2009.
13. Wang, J. P., B. Z. Wang, Y. X. Wang, and Y. X. Guo, "Dual-band microstrip stepped-impedance bandpass filter with defected ground structure," *Journal of Electromagnetic Waves and Applications*, Vol. 22, No. 4, 463–470, 2008.
14. Liu, A.-S., T.-Y. Huang, and R.-B. Wu, "A dual wideband filter design using frequency mapping and stepped-impedance resonators," *IEEE Trans. Microwave Theory Tech.*, Vol. 56, No. 12, 2921–2929, December 2008.
15. Chin, K.-S. and J.-H. Yeh, "Dual-wideband bandpass filter using short-circuited stepped-impedance resonators," *IEEE Microw. Wireless Comp. Lett.*, Vol. 19, No. 3, 155–157, March 2009.
16. Chen, H. and Y. X. Zhang, "Dual-band filter using composite microstrip/CPW structure," *Electronics Letters*, Vol. 44, No. 16, 979–980, July 2008.
17. Weng, M. H., C. T. Liaug, H. W. Wu, S. R. Vargas, and R. Y. Yang, "A compact microstrip dual-wideband bandpass filter using ladder stub resonator," *Microw. Opt. Technol. Lett.*, Vol. 51, No. 6, 1391–1393, June 2009.
18. Wang, X.-H., B.-Z. Wang, and K. J. Chen, "Compact broadband dual-band bandpass filters using slotted ground structures," *Progress In Electromagnetics Research*, Vol. 82, 151–166, 2008.
19. Gong, J.-Q. and Q.-X. Chu, "SCRLH TL based UWB bandpass

filter with widened upper stopband," *Journal of Electromagnetic Waves and Applications*, Vol. 22, No. 14–15, 1985–1992, 2008.

20. Lin, W. J., J. Y. Li, D. B. Lin, L. S. Chen, and M. P. Houng, "Miniaturized wideband ring-type bandpass filters with upper stopband characteristic," *Journal of Electromagnetic Waves and Applications*, Vol. 24, No. 7, 931–939, 2010.
21. Gao, S. S., S. Q. Xiao, J. P. Wang, X. S. Yang, Y. X. Wang, and B. Z. Wang, "A compact UWB bandpass filter with wide stopband," *Journal of Electromagnetic Waves and Applications*, Vol. 22, No. 8–9, 1043–1049, 2008.
22. Shaman, H. and J.-S. Hong, "A novel ultra-wideband (UWB) bandpass filter (BPF) with pairs of transmission zeroes," *IEEE Microw. Wireless Comp. Lett.*, Vol. 17, No. 2, 121–123, February 2007.
23. Thomson, N. and J.-S. Hong, "Compact ultra-wideband microstrip/coplanar waveguide bandpass filter," *IEEE Microw. Wireless Comp. Lett.*, Vol. 17, No. 3, 184–186, March 2007.
24. Song, K. and Q. Xue, "Novel broadband bandpass filters using Y-shaped dual-mode microstrip resonators," *IEEE Microw. Wireless Comp. Lett.*, Vol. 19, No. 9, 548–550, September 2009.
25. Kuo, T.-N., C.-H. Wang, and C. H. Chen, "A compact ultra-wideband bandpass filter based on split-mode resonator," *IEEE Microw. Wireless Comp. Lett.*, Vol. 17, No. 12, 852–854, December 2007.
26. Makimoto, M. and S. Yamashita, *Microwave Resonators and Filters for Wireless Communications-theory and Design*, Springer-Verlag, Berlin, Germany, 2001.
27. Chen, F.-C. and Q.-X. Chu, "A compact dual-band bandpass filter using pseudo-interdigital E-shaped SIRs," *Cross Strait Tri-Regional Radio Science and Wireless Technology Conference*, 444–446, 2008.
28. Li, R. and L. Zhu, "Compact UWB bandpass filter using stub-loaded multiple-mode resonator," *IEEE Microw. Wireless Comp. Lett.,* Vol. 17, No. 1, 40–42, January 2007.